PERGAMON

International Journal of Heat and Mass Transfer 46 (2003) 15–22

International Journal of HEAT and MASS TRANSFER

www.elsevier.com/locate/ijhmt

A heat transfer model for deep penetration laser welding based on an actual keyhole

Xiangzhong Jin *, Lijun Li, Yi Zhang

Laser Institute of Hunan University, Changsha, Hunan Province, 410082, China

Received 17 May 2002; received in revised form 3 July 2002

Abstract

Using a specially designed experimental setup, we obtained a clear stable keyhole with a high-speed camera. A heat transfer model with a cylindrical surface heat source has been developed under the assumption of the keyhole per thin layer being cylindrical. The model is numerically solved by finite element method, the temperature field around the keyhole and the heat flux lost to the keyhole wall can be obtained. The effects of such factors as the shape and the size of the keyhole, the welding speed on the shape of the melt pool are studied. By comparing the laser intensity absorbed on the keyhole walls with the heat flux lost there, the mechanism of energy balance on the keyhole walls is investigated.

1. Introduction

In deep penetration laser welding, when a laser beam with high intensity irradiates, a keyhole is formed in the workpiece, which enables the laser beam to penetrate deeply into the workpiece. Keyhole formation is the base of laser penetration welding. Hence, many papers [1–12] have been published to deal with this aspect, and various keyhole models have been established, in which some special assumptions such as rotational symmetrical keyhole shapes with a straight center line have been given. These assumptions restrict these models to low welding speeds.

As well known, in practical deep penetration laser welding, especially in high-speed laser penetration welding, not only the keyhole shape is not rotational symmetry, but also its center line is not straight. The actual keyhole is bent in the opposite direction of the welding speed. Because it is difficult to observe the keyhole in welding processes, only a few experimental works have been done to identify the keyhole shape up till now. Arata et al. [13] did some pioneer experimental works in this aspect. They observed keyhole shapes in soda-lime glass using direct photographing and in metals using X-ray imaging technique, as shown in Fig. 1(a) and (b) respectively. We can find in Fig. 1(a) that the keyhole is not stable and the picture is not clear. These problems may be caused by two reasons. One is that the 150 W laser power and the 1 mm/s welding speed they used are too low, the other is that it is difficult to distinguish the keyhole from the high-temperature emission region. But in the photograph of Fig. 1(b), another problem exists, as they pointed out that, "the contrast of the radiographs was too low to understand the deep penetration mechanism".

In this paper, the keyhole shape of laser welding glass was experimentally observed, and a heat transfer model was established thereby. The numerical solutions were obtained by means of finite element method, both the temperature distribution around the keyhole and the heat flux lost on the keyhole wall have been calculated, from which the effects of such factors as the welding speeds, the keyhole diameters on laser welding are discussed. By comparing the heat flux loss of the model on the keyhole wall with the laser intensity absorbed on the wall, an important conclusion about how energy balance theory works on the keyhole wall has been drawn.

* Corresponding author. Tel.: +86-731-880-1236; fax: +86-731-890-1283.

E-mail address: jxz9000@hotmail.com (X. Jin).

0017-9310/03/$ - see front matter
PII: S0017-9310(02)00255-7

Nomenclature

$a1$–$a4$	polynomial coefficients of the keyhole front wall	T_s	temperature of the solid, K
$b1$–$b4$	polynomial coefficients of the keyhole rear wall	c_l	heat capacity of the liquid, $J\,kg^{-1}\,K^{-1}$
x, y, z	Cartesian coordinate, m	c_s	heat capacity of the solid, $J\,kg^{-1}\,K^{-1}$
Δz	thickness of the thin layer, m	ρ	density of the material, $kg\,m^{-3}$
$r_{kz}(z)$	keyhole radius at the depth of z, m	p	pressure in the liquid region, $N\,m^{-2}$
$x_z(z)$	distance between the beam axis and the keyhole center at the depth of z, m	T_a	the environmental temperature, K
u_x, u_y	liquid velocity components in x- and y-direction, m/s	r, θ	polar coordinates defined in Fig. 5
U	welding speed, m/s	T_v	vaporization temperature of the material, K
k_l	conductivity of the liquid, $W\,m^{-1}\,K^{-1}$	u_θ	velocity component in the local tangential direction
k_s	conductivity of the solid, $W\,m^{-1}\,K^{-1}$	T_m	melting temperature of the material, K
T_l	temperature of the liquid, K	h_{sl}	heat of fusion of the material, $J\,kg^{-1}\,K^{-1}$
		θ_n	the angle between the x-axis and the local normal to the solid–liquid interface, rad

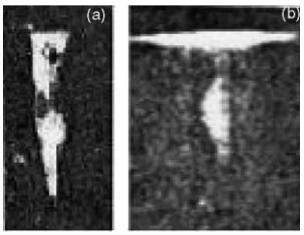

Fig. 1. Composite photograph of keyholes taken by Arata's group.

2. Experimental observation of keyhole profile

In order to get a clear keyhole, we recently improved the technique of laser welding glass. The experimental setup is shown in Fig. 2. The laser beam is focused by a GaAs lens with a focal length of 100 mm. A coaxial compressed air is used to protect the lens and an argon jet as the shielding gas. A high-speed camera is used to take the photos, the exposure of which is 1/1000 s, so both the laser beam and the keyhole can be treated as stationary in such a short period. In order to attenuate the high-temperature emission, a welding glass is placed between the camera and the sample. After testing various specifications of glass, GG17 (a Chinese brand similar to Pyrex) glass with excellent heat-resistance and a great deal of differences between the softening point and the vaporization point was chosen as the sample material at last. All the surfaces of the samples were polished before welding.

The laser used was a home made 1000 W CO_2 CW laser with a folded resonator. The transverse mode of the output beam is near Gaussian.

Using this setup, a clear picture of typical keyhole has been obtained as shown on Fig. 3(a). The welding conditions were as follows: laser beam power: 600 W,

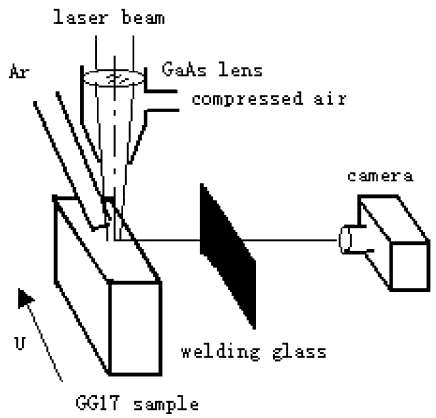

Fig. 2. Experimental setup.

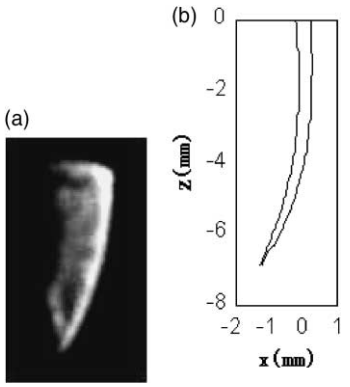

Fig. 3. Typical keyhole picture.

beam diameter before focusing: 15 mm, welding speed: 10 mm/s. From the above picture, we may deduce that the keyhole shape is nearly conical, its vertex angle decreases as keyhole depth increases. When the keyhole is deep enough, the keyhole diameter at different depth varies little. In this case, the keyhole can be treated as a cylinder. Moreover, the keyhole is bent in the opposite direction of the welding speed. Around the keyhole, especially at the rear part, there is a less bright region, which is the high-temperature emission region. At this moment, we are not sure if it is the melt pool or not, as the glass has no definite melting point.

Based on the above actual keyhole, a heat transfer model can be constructed to calculate the temperature distribution around the keyhole, then the heat flux lost on the keyhole wall can also be conducted.

3. Heat transfer model

In order to construct the model, the following assumptions must be given:

(1) The heat transfer and the fluid flow along the laser beam axis z are neglected, and the heat transfer problem becomes a two-dimension one.
(2) For any depth of z, the keyhole is treated as a circle (cylinder), but its diameter and the center position change with z.
(3) The temperature on all the keyhole wall is assumed to be the vaporization temperature of the material, but the vaporization energy of a small part of the material is neglected.
(4) No convective heat loss on the sample surface is considered.
(5) Homogeneous, isotropic and temperature-dependent properties are assumed both in solid region and in liquid region, but the density in the liquid region is assumed to be constant.
(6) The molten liquid is assumed to be Newtonian and incompressible.
(7) The coordinate origin is fixed at the keyhole center and a quasi-stable process is considered.

As the clear keyhole shape has already been got, the positions of the keyhole front and the rear walls can be measured and expressed by the method of polynomial fitting as follows:

For the front wall

$$x = f_f(z) = a_1 z^3 + a_2 z^2 + a_3 z + a_4 \tag{1}$$

For the rear wall

$$x = f_r(z) = b_1 z^3 + b_2 z^2 + b_3 z + b_4 \tag{2}$$

where $a1$–$a4$, $b1$–$b4$ are the polynomial coefficients of the keyhole front and rear wall, respectively.

Under the assumption (2), the actual keyhole can be treated as combination of a series of thin layers with the thickness of Δz, as shown in Fig. 4. In each thin layer, the problem can be treated as a two-dimensional one.

The keyhole radius at the depth of z can be expressed as

$$r_{kz}(z) = \frac{f_f(z) - f_r(z)}{2} \tag{3}$$

The distance between the beam axis and the keyhole center at this depth is

$$x_z(z) = r_{kz}(z) - f_f(z) \tag{4}$$

Pick a thin layer from the depth of z. Under the above assumptions, the governing equations of this layer in Cartesian coordinate as shown in Fig. 5 can be expressed as follows:

In the liquid region, the continuity equation

$$\frac{\partial u_x}{\partial x} + \frac{\partial u_y}{\partial y} = 0 \tag{5}$$

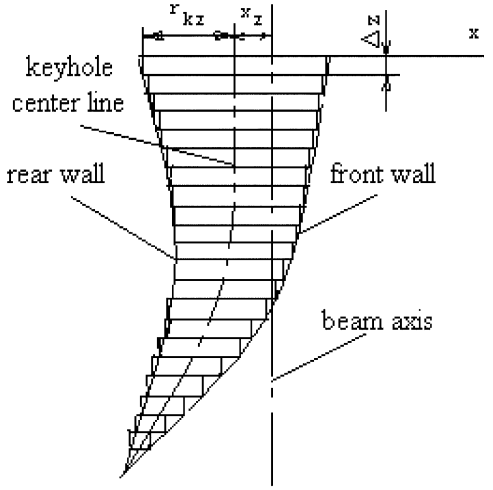

Fig. 4. A diagram of the resolution of the keyhole.

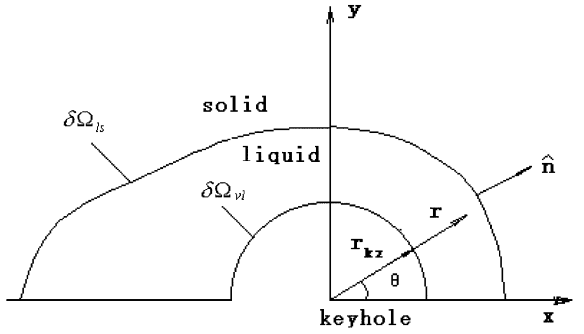

Fig. 5. A thin layer of the keyhole.

momentum equation in x-direction

$$\rho u_x \frac{\partial u_x}{\partial x} + \rho u_y \frac{\partial u_x}{\partial y} = -\frac{\partial p}{\partial x} + \frac{\partial}{\partial x}\left(2\mu \frac{\partial u_x}{\partial x}\right) + \frac{\partial}{\partial y}\left[\mu\left(\frac{\partial u_x}{\partial y} + \frac{\partial u_y}{\partial x}\right)\right] \tag{6}$$

momentum equation in y-direction

$$\rho u_x \frac{\partial u_y}{\partial x} + \rho u_y \frac{\partial u_y}{\partial y} = -\frac{\partial p}{\partial y} + \frac{\partial}{\partial y}\left(2\mu \frac{\partial u_y}{\partial y}\right) + \frac{\partial}{\partial x}\left[\mu\left(\frac{\partial u_x}{\partial y} + \frac{\partial u_y}{\partial x}\right)\right] \tag{7}$$

energy equation

$$\frac{\partial}{\partial x}\left(k_\mathrm{l} \frac{\partial T_\mathrm{l}}{\partial x}\right) + \frac{\partial}{\partial y}\left(k_\mathrm{l} \frac{\partial T_\mathrm{l}}{\partial y}\right) - \rho u_x \frac{\partial (c_\mathrm{l} T_\mathrm{l})}{\partial x} - \rho u_y \frac{\partial (c_\mathrm{l} T_\mathrm{l})}{\partial y} = 0 \tag{8}$$

In the solid region, energy equation

$$\frac{\partial}{\partial x}\left(k_\mathrm{s} \frac{\partial T_\mathrm{s}}{\partial x}\right) + \frac{\partial}{\partial y}\left(k_\mathrm{s} \frac{\partial T_\mathrm{s}}{\partial y}\right) - \rho U \frac{\partial (c_s T_\mathrm{s})}{\partial x} = 0 \tag{9}$$

where x and y are the axes of the coordinate system defined in Fig. 5; u_x and u_y are the liquid velocity components in x- and y-direction; U is the welding speed; k_l is the conductivity of the liquid; k_s is the conductivity of the solid; T_l is the temperature of the liquid; T_s is the temperature of the solid; c_l is the heat capacity of the liquid; c_s is the heat capacity of the solid; ρ is the density of the material; p is the pressure in the liquid region.

The boundary conditions related to the above governing equations can be mathematically stated as follows:

(1) On the symmetrical plane, i.e. at $y = 0$,

$$\frac{\partial u_x}{\partial y} = 0; \quad u_y = 0; \quad \frac{\partial T_\mathrm{l}}{\partial y} = 0; \quad \frac{\partial T_\mathrm{s}}{\partial y} = 0 \tag{10}$$

(2) As $x \to \pm\infty$ or $y \to \infty$,

$$T_\mathrm{s} = T_\mathrm{a} \tag{11}$$

where T_a is the environmental temperature.

(3) Because the liquid material cannot flow across the keyhole wall ($\delta\Omega_{vl}$ in Fig. 5), its velocity component in the local normal direction is zero, i.e. at $r = (x^2 + y^2)^{1/2} = r_{kz}(z)$,

$$u_r = u_x \cos\theta + u_y \sin\theta = 0 \tag{12}$$

where r and θ are the polar coordinates defined in Fig. 5.

(4) At $r = (x^2 + y^2)^{1/2} = r_{kz}(z)$,

$$T_\mathrm{l} = T_\mathrm{v} \tag{13}$$

where T_v is the vaporization temperature of the material.

(5) Because the laser beam cannot resist the sideflow of the liquid material, the tangential shear stress of the liquid at the keyhole surface is also zero, i.e. at $r = (x^2 + y^2)^{1/2} = r_{kz}(z)$,

$$\frac{\partial}{\partial r}\left(\frac{u_\theta}{r}\right) = 0 \tag{14}$$

where u_θ is the velocity component in the local tangential direction.

(6) On the solid–liquid interface ($\delta\Omega_\mathrm{ls}$ in Fig. 5), the no-slip condition and the local energy balance exist, i.e. on $\delta\Omega_\mathrm{ls}$

$$u_x = U; \quad u_y = 0 \tag{15}$$

$$T_\mathrm{l} = T_\mathrm{s} = T_\mathrm{m} \tag{16}$$

$$-\frac{\partial (k_\mathrm{s} T_\mathrm{s})}{\partial n} = -\frac{\partial (k_\mathrm{l} T_\mathrm{l})}{\partial n} + \rho U h_\mathrm{sl} \cos\theta_n \tag{17}$$

where T_m is the melting temperature of the material; h_sl is the heat of fusion; θ_n is the angle between the x-axis and the local normal to the solid–liquid interface.

4. Results and discussion

The above model can be numerically solved using a finite element software ANSYS, some useful results have been got.

The keyhole shown in Fig. 3(a) are taken as an example to be calculated. In this case, the polynomial coefficients of the front and rear keyhole wall are as follows (x and z all in meters): $a1 = 6366$, $a2 = 12.3057$, $a3 = 0.0002476$, $a4 = 0.0002214$, $b1 = 2370$, $b2 = -19.8091$, $b3 = 0.0916$, $b4 = -0.0002233$. The fitting keyhole profile is shown in Fig. 3(b), which can be used for further theoretical study.

Fig. 6 shows the temperature distribution around the keyhole on the surface of the workpiece. Because the conductivity of GG17 glass is very small, the temperature gradient around the keyhole is very big. Furthermore, as there is a relative welding speed between the workpiece and the laser beam, the temperature gradient near the front wall of the keyhole is much greater than that near the rear wall of the keyhole.

Fig. 7 shows the melt pool shape around the keyhole on the surface of the workpiece. The melt pool is enlarged in the opposite direction of the welding speed because of the welding speed. The part of the melt pool in front of the keyhole is very thin, while most part of the melt pool is located behind the keyhole.

Similarly, we can get all the melt pool shapes around the keyhole from the top to the bottom of the keyhole, then the melt pool profile in the symmetrical plane along the moving direction can be obtained, as shown in Fig. 8. Compared the calculated melt pool profile with the

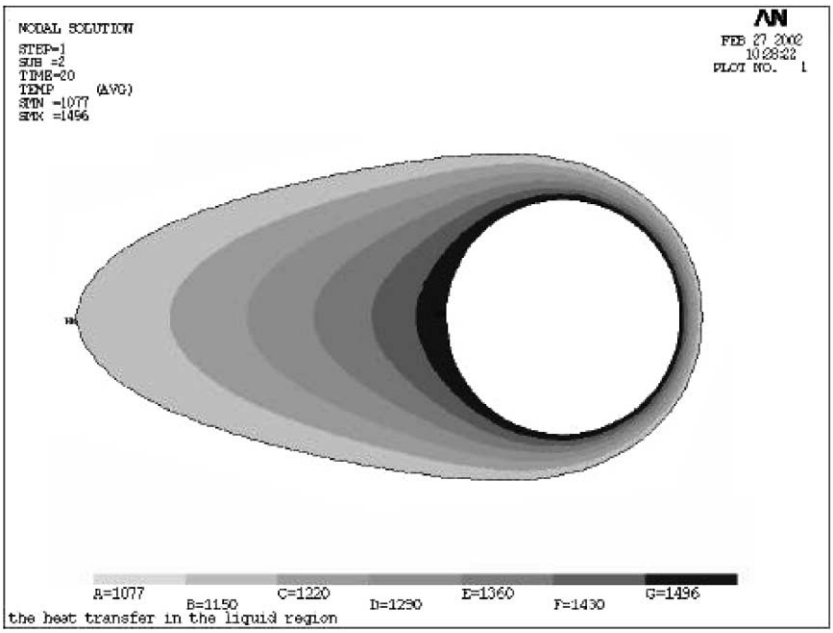

Fig. 6. Temperature distribution on the workpiece surface.

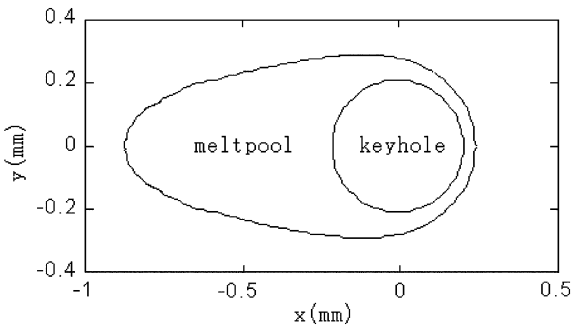

Fig. 7. Melt pool shape on the workpiece surface.

the less bright region, which can be measured from the keyhole picture shown on Fig. 3(a), we can find that there is some difference between the two profiles. As a result, we guess that the less bright region around the keyhole is not only the melt pool, it is actually the high-temperature emission region.

We can calculate the heat flux lost on the front and rear wall of the keyhole, as shown in Fig. 9. It can be seen that the heat flux lost on the front wall is one order greater than that lost on the rear wall.

As well known, two mechanisms of Fresnel absorption and inverse Bremsstrahlung absorption usually exist in deep penetration laser welding. However, because the main composition of glass GG17 is SiO_2, the ionization energy of which is very high, it is difficult to form plasma and the vapor of the glass material is transparent to the CO_2 laser beam. As a result, the only beam absorption mechanism in the keyhole is Fresnel absorption.

When a Gaussian beam enters a keyhole, part of it is cut and a Gaussian beam no longer exists. Its behavior in the keyhole can be calculated with geometrical optics. In order to model the beam's behavior, we suggest that all the Gaussian beam is focused at the focal point of the lens, but the focal point is 2.5 mm above the sample surface, so that the beam diameter at the surface is about 0.38 mm, which equals to the focused Gaussian beam diameter. The distance between the beam axis and the keyhole center at this depth is 0.02 mm. Under the above conditions, the laser intensity absorbed on the front and rear wall of the keyhole through Fresnel absorption can be calculated by tracing a light beam (the calculation details can be seen in Ref. [14]), which is also shown in Fig. 9. It can be seen that for the front wall, there is a high and pretty uniform power density distributed along the wall; but for the rear wall, only some weak power densities distributed in some individual regions, most part of which has even no any beam illumination.

Comparing the heat flux lost on the keyhole wall with the laser intensity absorbed on the same keyhole wall, it can be seen that even though there is a difference between the two values obtained, but considering the approximation of the calculation, we can deduce that there should be an energy balance between the absorbed laser intensity and the lost heat flux at each point of the front wall of a keyhole, and the laser intensity must be high enough to heat, melt and vaporize the front material. However, at most points of the rear wall, a strange

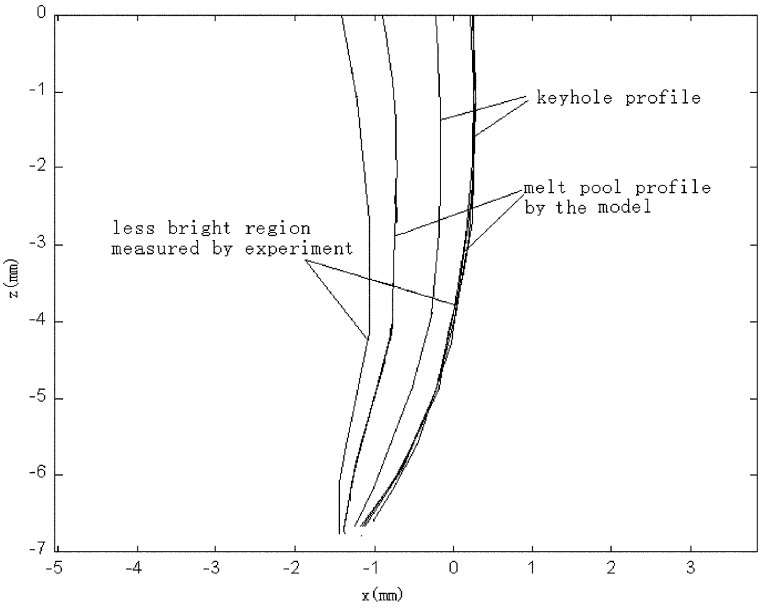

Fig. 8. Melt pool profile in the symmetrical plane along the moving direction.

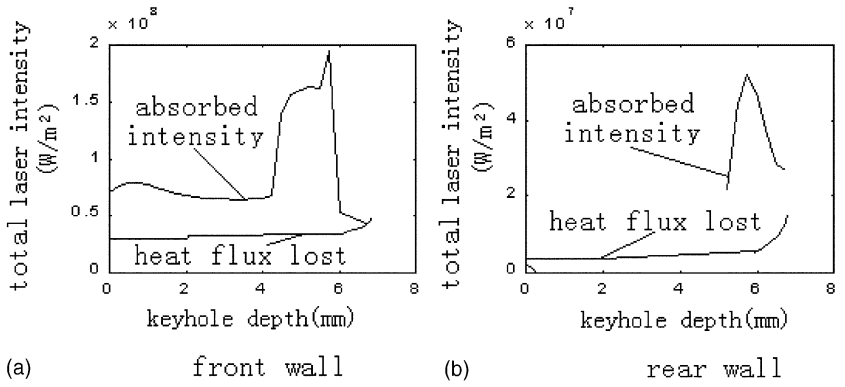

Fig. 9. Laser intensity absorbed and heat flux lost on the front and rear walls of the keyhole.

phenomenon occurs, i.e. there is only heat flux lost but no laser intensity absorbed. Now, such a question is raised: How does the energy balance work on the rear keyhole wall?

In order to answer the above question, we have studied the role of the convection flow in the melt pool, and have obtained the velocity field in the melt pool on the sample surface, which is shown in Fig. 10. It can be seen that there is a strong convection flow forced by the surface tension in the melt pool, the maximum flow velocity of which is 10 times or so as the welding speed. As P.G. Klemens [11] pointed out that in deep penetration laser welding, only a little of the melt material passed through the keyhole wall and then was vaporized to form the ablation pressure that kept the keyhole open, most of the melt material flew from the front of the melt pool to the rear of the melt pool around the keyhole. It is just the strong convection flow of the melt material that brings the heat from the front of the melt pool to the rear of the melt pool to balance the heat flux loss on the rear wall of the keyhole.

Using the model proposed, we have also got the melt pool shapes at different welding speeds, as shown in Fig. 11. The keyhole diameter is assumed to be 0.32 mm. The numbers in Fig. 11 represent the welding speeds (in mm/min). With the welding speed increasing, the length of the melt pool increases, but the width of the melt pool decreases.

We can also calculate the variation of the melt pool shapes with the keyhole diameter. Fig. 12 shows the melt

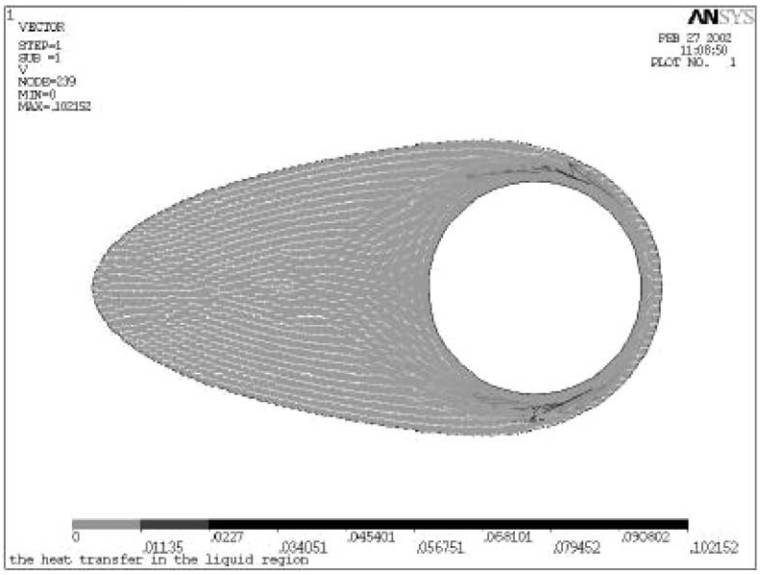

Fig. 10. Flow field on the workpiece surface.

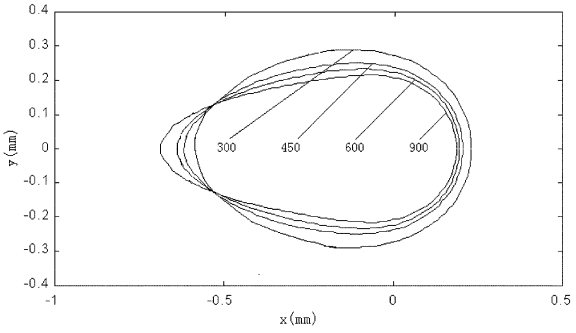

Fig. 11. Melt pool shapes at different welding speeds.

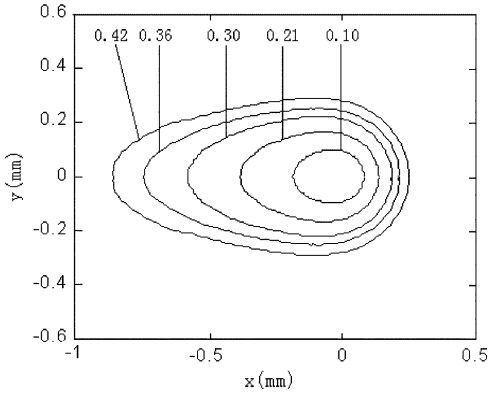

Fig. 12. Melt pool shapes on the workpiece surface at different keyhole diameters.

pool shapes at different keyhole diameters. The welding speed used is 600 mm/min. The numbers in Fig. 12 represent the keyhole diameters. With the keyhole diameter increasing, not only the length of the melt pool increases, but also the width of the melt pool increases too.

5. Conclusion

From the above discussion, the following conclusions can be drawn:

(1) Under certain conditions, a stable and clear keyhole can be observed in laser welding of glass GG17 (Pyrex). This offers an effective way to analyze the keyhole behavior in laser welding process.
(2) The keyhole is bent in the opposite direction of the welding speed and cone shaped. When the keyhole is deep enough, it can be treated as a cylinder.
(3) Plasma is difficult to form in laser welding glass because of its high ionization energy, the main absorption mechanism in the keyhole is the Fresnel absorption.
(4) The energy balance theory works in different manners on different walls of the keyhole. On the front wall of the keyhole, there is an energy balance between the laser intensity absorbed through Fresnel absorption and the heat flux loss due to conduction and convection. However, on the rear wall of the keyhole, there are only some weak power densities distributed in some individual regions, most part of the rear wall has no any beam illumination. In order to keep the energy balance there, the energy needed is brought from the front part to the rear part of the melt pool by convection.

References

[1] P. Berger, Physical models on deep penetration welding with emphasis on fluid dynamics, in: Gas Flow and Chemical Lasers, SPIE, Vol. 1810, 1992, pp. 554–561.
[2] J. Mazumder, An overview of melt dynamics in laser processing, in: High Power Lasers, SPIE, Vol. 801, 1987, pp. 228–241.
[3] R. Peretz, Workpiece temperature distribution for deep penetration welding with high energy focused beam, Optics Lasers Eng. 7 (1986/87) 69–81.
[4] A. Kaplan, A model of deep penetration laser welding based on calculation of the keyhole profile, J. Phys. D: Appl. Phys. 27 (1994) 1805–1814.
[5] W.M. Steen, J. Dowden, M. Davis, P. Kapadia, A point and line source model of laser keyhole welding, J. Phys. D: Appl. Phys. 21 (1988) 1255–1260.
[6] R. Akhter, M. Davis, J. Dowden, P. Kapadia, M. Ley, W.M. Steen, A method for calculating the fused zone profile of laser keyhole welds, J. Phys. D: Appl. Phys. 21 (1989) 23–28.
[7] J. Dowden, P. Kapadia, A mathematical investigation of the penetration depth in keyhole welding with continuous CO_2 lasers, J. Phys. D: Appl. Phys. 28 (1993) 2252–2261.
[8] K.N. Lankalapalli, J.F. Tu, M. Gartner, A model for estimating penetration depth of laser welding processes, J. Phys. D: Appl. Phys. 29 (1996) 1831–1841.
[9] T. Miyazaki, W.H. Giedt, Heat transfer from an elliptical cylinder moving through an infinite plate applied to electron beam welding, Int. J. Heat Mass Transfer 25 (1982) 807–814.
[10] M. Baeva, P. Baev, A. Kaplan, An analysis of the heat transfer from a moving elliptical cylinder, J. Phys. D: Appl. Phys. 30 (1997) 1190–1196.
[11] P.G. Klemens, Heat balance and flow conditions for electron beam and laser beam, J. Appl. Phys. 47 (5) (1976) 2165–2174.
[12] J. Dowden, N. Postacioglu, M. Davis, P. Kapadia, A keyhole model in penetration welding with a laser, J. Phys. D: Appl. Phys. 20 (1987) 36–44.
[13] Y. Arata, N. Abe, T. Oda, Fundamental phenomena in high power CO_2 laser welding (report I & II), Trans. JWRI 14 (1&2) (1985).
[14] X. Jin, A Theoretical and Experimental Study on Keyhole Effects in Laser Deep Penetration Welding, Ph.D Thesis, Hunan University, China, 2002.